ACS OMEGA

Article

Cite This: ACS Omega 2018, 3, 9880−9887

http://pubs.acs.org/journal/acsodf

From Complex Inorganic Oxides to Ag−Bi Nanoalloy: Synthesis by Femtosecond Laser Irradiation

Thales R. Machado,[†] Nadia G. Macedo,[†] Marcelo Assis,[†] Carlos Doñate-Buendia,[‡] Gladys Mínguez-Vega,[‡] Mayara M. Teixeira,[†] Camila C. Foggi,[†] Carlos E. Vergani,[⊥] Héctor Beltrán-Mir,[§] Juan Andrés,[∥] Eloisa Cordoncillo,[§] and Elson Longo*[,†]

[†]Departamento de Química, CDMF, Universidade Federal de São Carlos (UFSCar), São Carlos 13565-905, São Paulo, Brazil

[‡]Institut de Noves Tecnologies de la Imatge (INIT), GROC, [§]Departament de Química Inorgànica i Orgànica, and [∥]Departament de Química Física i Analítica, Universitat Jaume I (UJI), Castellón de la Plana 12071, Castelló, Spain

[⊥]Faculdade de Odontologia, Universidade Estadual Paulista (UNESP), Araraquara 14801-385, São Paulo, Brazil

Supporting Information

ABSTRACT: Bimetallic nanoalloys with a wide variety of structures and compositions have been fabricated through many diverse techniques. Generally, various steps and chemicals are involved in their fabrication. In this study, the synthesis of Ag−Bi nanoalloys by femtosecond laser irradiation of an inorganic oxide $Ag_2WO_4/NaBiO_3$ target without any chemicals like reducing agents or solvent is presented. The interaction between these materials and the ultrashort pulse of light allows the migration of Ag and Bi atoms from the crystal lattice to the particles surfaces and then to the plasma plume, where the reduction of the positively charged Ag and Bi species in their respective metallic species takes place. Subsequently, the controlled nucleation and growth of the Ag−Bi alloyed nanoparticles occurs in situ during the irradiation process in air. Although at the bulk level, these elements are highly immiscible, it was experimentally demonstrated that at nanoscale, the Ag−Bi nanoalloy can assume a randomly mixed structure with up to 6 ± 1 atom % of Bi solubilized into the face-centered cubic structure of Ag. Furthermore, the Ag−Bi binary system possesses high antibacterial activity against *Staphylococcus aureus* (methicillin-resistant and methicillin-susceptible), which is interesting for potential antimicrobial applications, consequently increasing their range of applicability. The present results provide potential insights into the structures formed by the Ag−Bi systems at the nanoscale and reveal a new processing method where complex inorganic oxides can be used as precursors for the controlled synthesis of alloyed bimetallic nanoparticles.

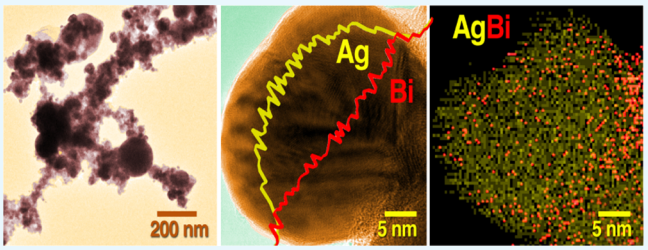

1. INTRODUCTION

Nanoalloys (NAs) composed of different metals are of broad scientific interest mainly because they combine the properties of single-metal nanoparticles (NPs) and generally present unique properties not found in the NPs of the two metals individually.[1,2] NAs composed of Ag, Au, Bi, Co, Cu, Ni, Pd, Pt, Sb, and other metals exhibit new functions because of the synergistic rather than merely additive effects of the two distinct metals, leading to markedly enhanced physical and chemical properties. This fact enables their widespread applications in various fields, such as catalysis, electronics, photonics, and biomedicine.[3−16] These technological applications are mainly dependent on the chemical composition, morphology, and size of the NAs.[2,17] Moreover, the properties of bimetallic NAs also depend on their complex structures, in which the atomic arrangements can be classified into four mixing patterns: core−shell, multishell, and subcluster ("Janus" particles) segregated patterns or a mixed structure (ordered or a randomly mixed solid solution).[18]

Although the goal of obtaining bimetallic NAs is very attractive, it has been proven to be difficult to achieve when two immiscible metals are targeted. However, two elements which do not have a significant miscibility gap in their phase diagram at the bulk level can form alloys at the nanoscale.[19−21] Ag−Bi NA is a clear example. The very low solubility between Ag and Bi elements, with less than ∼3 atom % of Bi solubilizing in Ag matrix (solid solution) and no detectable solubility of Ag in Bi in the bulk scale,[22,23] is due to their different crystalline structures, i.e., face-centered cubic (fcc) for Ag^0 ($fm3m$) and rhombohedral for Bi^0 ($R3m$) at atmospheric conditions.[24] At the nanoscale, Ag−Bi alloyed NPs have been stabilized with coexisting bulklike lattices of Ag^0 and Bi^0 in the same particle (stack of nanodomains) or a segregated pattern, depending on the synthesis conditions of the soft chemical route (temperature < 200 °C).[25−27] The Ag−Bi NA is an emerging material that has attracted recent interest due to its superior photocatalytic production of H_2 via water splitting,[25] degradation of organic pollutants in wastewater,[26] and

Received: June 6, 2018
Accepted: August 13, 2018
Published: August 24, 2018

DOI: 10.1021/acsomega.8b01264
ACS Omega 2018, 3, 9880−9887

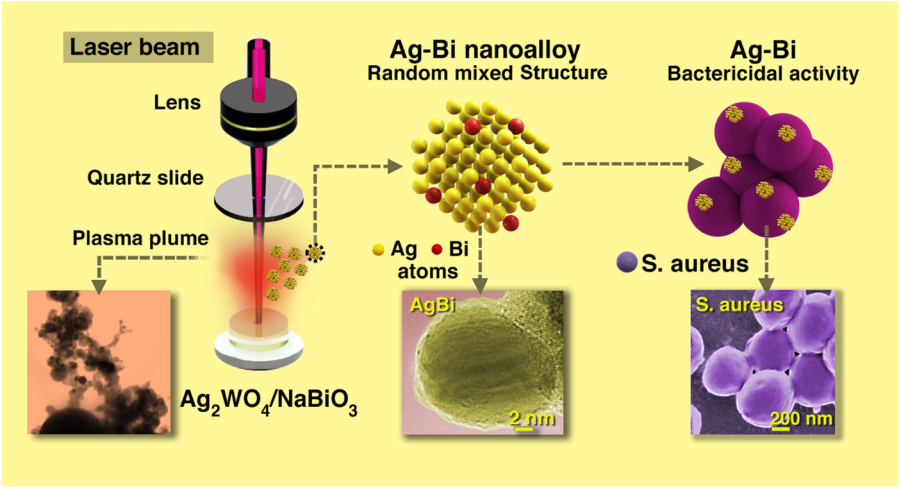

Figure 1. Representation of the procedure employed to obtain Ag−Bi NAs by fs laser irradiation on a $Ag_2WO_4/NaBiO_3$ target, where the generation of the plasma plume takes place (left). Irregular spheres of Ag−Bi alloyed NPs are sensed (center), presenting a randomly mixed pattern (solid solution) of Bi atoms in Ag structure. Ag−Bi NAs present high bactericidal activity against *Staphylococcus aureus* (methicillin-resistant and methicillin-susceptible) (right). The digital micrographs illustrate, from left to right, the plasma plume generated, a single Ag−Bi alloyed NP, and an agglomerate of *S. aureus* bacteria.

decomposition of nitric oxide.[27] However, at present, there are only few published studies investigating other possible structures which can be formed in the Ag−Bi system at the nanoscale, such as pure solid solutions of Ag and Bi elements, and the potential applications of the resulting NAs.

Due to the extensive proliferation of femtosecond (fs) laser technology in recent years, the interaction of a molecular system with intense laser light has allowed an increasing number of researchers to investigate the appearance of unusual phenomena, such as melting, ablation, and recrystallization, leading to the stabilization of nonequilibrium or metastable phases with unique compositions, structures, and properties.[28−30] Irradiation of a mixture of single-element micro/nanomaterials may lead to their alloying and the fabrication of multielement structures, making this a top-down, efficient, versatile, surfactant-free, and low-cost approach for obtaining bimetallic NAs.[31−35] Thus, fabrication of NAs by fs laser irradiation can provide a green synthesis solution, in which no organic solvents or chemical reducing agents are needed.[36,37] However, to the best of our knowledge, there are no studies in the literature reporting the fabrication of Ag−Bi NAs by fs laser irradiation.

In this communication we seek to fulfill 2-fold objectives (Figure 1). The first is to report the novel formation of a Ag−Bi NA with nonconventional structure and composition stabilized at the nanoscale with a random mixture of up to 6 ± 1 atom % of Bi into the fcc structure of Ag via fs laser irradiation of a $Ag_2WO_4/NaBiO_3$ target. To support this finding, a detailed analysis of images obtained by advanced electron microscopy techniques, including field-emission scanning electron microscopy (FE-SEM), transmission electrons microscopy (TEM), high-resolution TEM (HR-TEM), scanning TEM (STEM), and energy-dispersive X-ray spectroscopy (EDS), has been performed. The second aim is to demonstrate that the as-synthesized Ag−Bi NA has an excellent bactericidal activity and contribute to broadening its possible applications.

2. RESULTS AND DISCUSSION

In the last few years, our research group has conducted several studies focused on the growth of monometallic NPs on surfaces of semiconductors for technological and biomedical applications of the resultant composites.[35,38−40] In this sense, we demonstrated theoretically and experimentally that Ag-based complex inorganic oxides are very suitable for the controlled synthesis of Ag^0 nanostructures with distinct sizes and shapes by their interaction with an electron beam.[35,39−45] Recently, we have reported how these structures can also be used as substrate for Ag^0 synthesis by fs laser irradiation, while Bi-based oxides can be used for the formation of Bi^0 NPs.[35,46] For the present study, we selected a combined substrate composed of Ag_2WO_4 microrods and $NaBiO_3$ nanoflakes as the sources of Ag^0 and Bi^0 nanoclusters, respectively. Hence, we aim to associate the recent advances of our current research works focused on the study of semiconductor (complex inorganic oxide) interactions with electrons and photons to demonstrate, for the first time, that a Ag−Bi NA can be prepared by fs laser irradiation. For a detailed description of the structural and morphological characteristics of the materials used, refer to Section S1 of the Supporting Information (SI).

The Ag_2WO_4 and $NaBiO_3$ materials possess significant lattice disorder, and by interacting with photons, the Ag and Bi species migrate from the crystal lattice to the particles surfaces and then to the plasma plume, where the reduction of the positively charged Ag and Bi species in their respective metallic species takes place. Since the reduction, nucleation, and growth of the Ag^0 and Bi^0 metallic structures occur in a controlled manner and in situ with the irradiation process in air, the reaction kinetics are compatible with the experimental conditions necessary for the formation of Ag−Bi NAs. Hence, the samples were ablated in air and the Ag−Bi NAs are expected to be formed in the plasma plume generated in the laser−matter interaction. In this plume, electrons and ions of the Ag and Bi coexist in extreme pressure and thermal conditions, which favors the formation of the alloy. When the

DOI: 10.1021/acsomega.8b01264
ACS Omega 2018, 3, 9880−9887

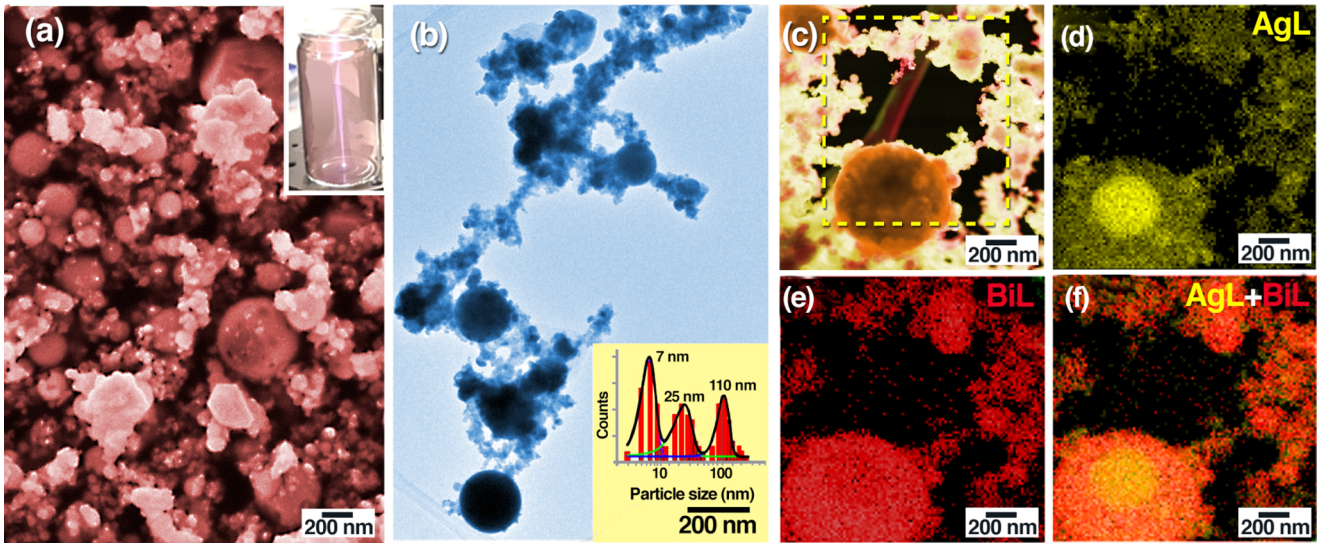

Figure 2. General view of the Ag−Bi alloyed NPs produced by fs irradiation: (a) FE-SEM image and a digital image (inset) illustrating the irradiation process of the $Ag_2WO_4/NaBiO_3$ target (bottle bottom) and the generation of Ag−Bi NAs (reddish plasma plume), (b) TEM image with an estimation of particle dimensions (inset), (c) BF-STEM image, (d) AgL EDS map, (e) BiL EDS map, and (f) AgL−BiL EDS map overlay evidencing a mixed pattern of these elements.

plasma cools down and disappears, it releases the nanoparticles in the air.

Figure 2a,b shows FE-SEM and TEM images, respectively, of the Ag−Bi NPs obtained by fs laser irradiation. As can be seen, spherical nanoparticles are present, which are typically observed in nanomaterials obtained by laser treatment.[31,34] These nanospheres have average sizes of 7, 25, and 110 nm, as shown Figure 2b (inset). Their composition was qualitatively studied by EDS mapping in the STEM imaging mode, and Figure 2c shows a bright-field STEM image (BF-STEM) of the analyzed region. The elemental distributions of Ag and Bi in this specific region are shown in Figure 2d,e, respectively. By overlaying these maps (Figure 2f), homogeneous Ag and Bi distributions were observed throughout almost all of the analyzed region, indicating the success of the synthesis procedure in obtaining a mixed Ag−Bi pattern. The elemental map also confirms that after fs laser irradiation, some spots in the samples are richer in either Ag (yellow regions) or Bi (red regions), as expected. This is because of the very limited solubility of Ag in the Bi crystalline structure and vice versa.

Figure 3a shows an HR-TEM image of an isolated monocrystalline particle of size 23 nm obtained by fs laser irradiation. The distance between the crystallographic planes present in this NP was measured, giving a value of 2.46 Å (inset), which can be indexed to the interplanar distance of the (111) family of planes in Ag^0 with the typical fcc structure, in agreement with the JCPDS database (PDF04-0783). An important feature is the difference between this value and the one obtained when measuring the crystallographic plane spacing in the pure Ag^0 sample prepared by fs irradiation of a Ag_2WO_4 target (2.36 Å for the (111) plane, a difference of about +4.2%, see Figure S3 in the SI), which agrees well with the reference data for this plane in Ag^0. This behavior is related to an expansion of the fcc crystalline lattice of metallic Ag^0 to accommodate Bi-substituting Ag atoms in the form of a randomly mixed pattern or solid solution (the atomic radii of Ag and Bi are 144 and 182 pm, respectively).[47] Moreover, the measured interplanar spacing in the Ag−Bi sample is very distinct from the values found for the orthorhombic crystalline

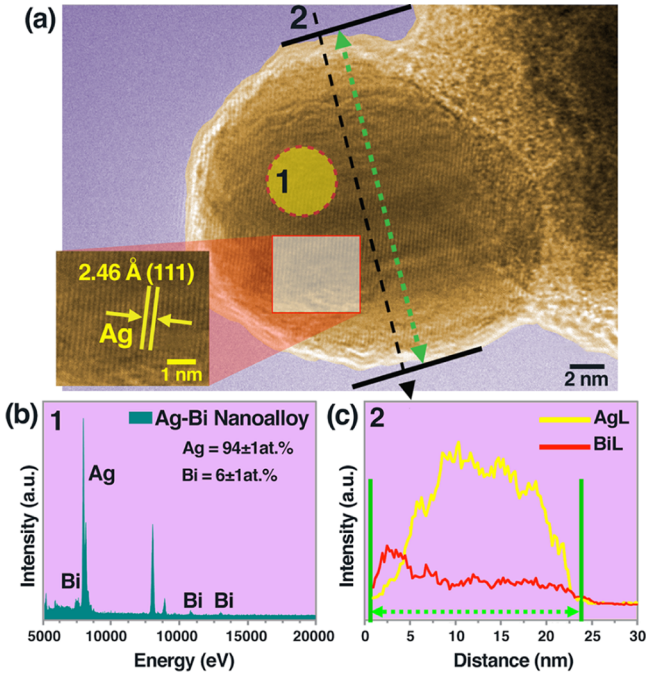

Figure 3. TEM characterization of a single Ag−Bi alloyed NP of size 23 nm. (a) HR-TEM image, (b) local EDS analysis of region 1, and (c) line EDS analysis of region 2.

structure of pure Bi^0 obtained by irradiating a $NaBiO_3$ target (see Figure S4 in the SI and the JCPDS database for this structure (44-12460)). This finding reinforces the conclusion that the Ag fcc structure was stabilized by the irradiation process in the Ag−Bi sample with Bi atoms inserted into the lattice in a doping level. To confirm the Ag−Bi NA formation, an EDS study was performed. The local analysis in region 1 (dashed circle) is shown in Figure 3b and confirms the major concentration of Ag element (94 ± 1 atom %), with the presence of Bi element at a doping level (6 ± 1 atom %). This result also indicates that Na or W has negligible concentration

DOI: 10.1021/acsomega.8b01264
ACS Omega 2018, 3, 9880−9887

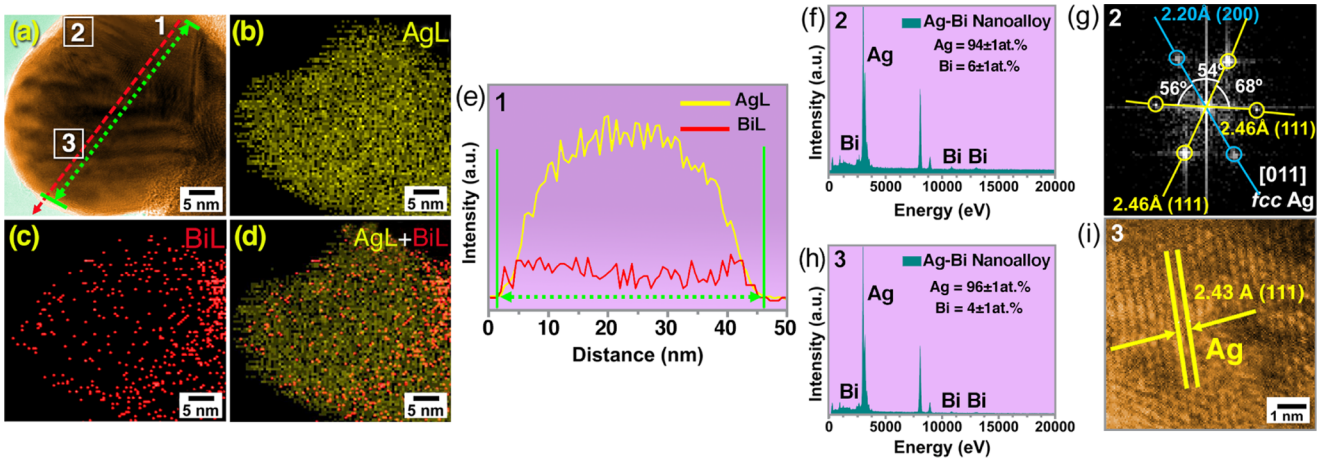

Figure 4. Insights into the formation of Ag−Bi NA. (a) HR-TEM images showing a monocrystalline Ag−Bi alloyed NP 43 nm in size, (b) AgL EDS map, (c) BiL EDS map, and (d) AgL−BiL overlaid EDS maps, and (e) line EDS profile of region 1. (f, g) Local quantification by EDS analysis and FFT of region 2 (NP border) and (h, i) local quantification by EDS analysis and HR-TEM images of region 3 (NP core).

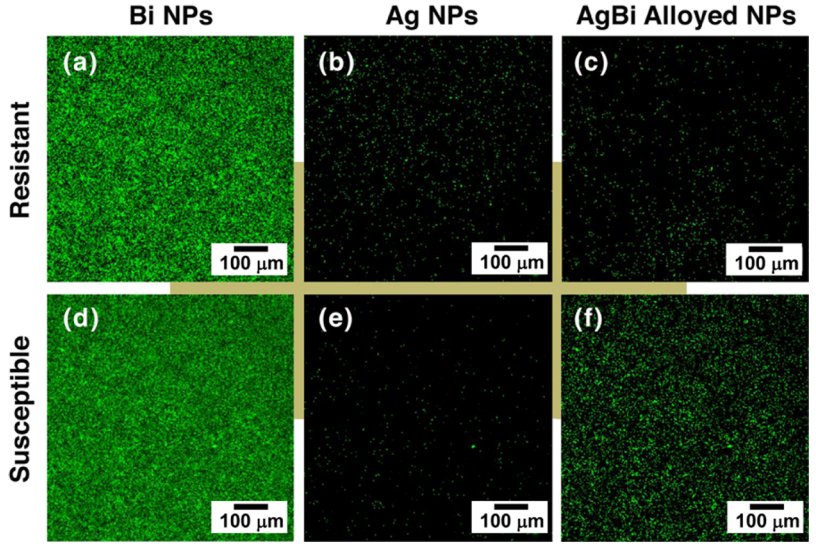

Figure 5. CLSM images of methicillin-resistant (top) and methicillin-susceptible (bottom) *S. aureus* cells treated with (a, d) Bi NPs, (b, e) Ag NPs, and (c, f) Ag−Bi NA.

in NPs analyzed at the plasma plume. The EDS line analysis (black dashed line 2) shown in Figure 3c demonstrates the distribution of Ag and Bi elements along the NP (green dotted line), indicating a homogeneous insertion of Bi atoms in the Ag structure. The slightly higher concentration of Bi at the surface of the NP (see the red line of BiL signal at Figure 3c) is explained by the low miscibility between Bi and Ag. Therefore, a very thin layer was formed, richer in Bi than the core of the Ag−Bi NP.

Figure 4a displays an HR-TEM image of a representative spot to gain a deeper insight into the Ag−Bi NAs formed by fs irradiation. As the figure shows, a faceted well-crystallized single particle of size 43 nm was detected. A qualitative elemental distribution by EDS mapping was performed by using the characteristic Lα lines of Ag and Bi. These results demonstrated a distribution with a major concentration of Ag element (yellow dots, Figure 4b) and also, to a lesser extent, Bi element (red dots, Figure 4c). By overlaying these two individual maps (Figure 4d), we concluded that the Bi element is well distributed throughout the NA with a higher concentration at the surface compared to the core. The line EDS analysis (red dashed line 1) of the Ag Lα and Bi Lα signals shown in Figure 4e also confirms the random mixture of Bi and Ag in the NA (green dotted line). The local EDS analysis in region 2, as illustrated in Figure 4f, indicates a composition of 94 ± 1 atom % Ag and 6 ± 1 atom % Bi, which is similar to the composition of NP shown in Figure 3. To get a deeper understanding, a fast Fourier transform (FFT) of this same region was realized (Figure 4g). In this image, the typical pattern of a cubic structure along the [011] axis zone is observed, which undoubtedly confirms the fcc structure of Ag. The (200) and (111) planes of cubic Ag^0 can be identified, in agreement with the JCPDS database (PDF04-0783), where an interplanar distance of 2.20 Å is present for the former and 2.46 Å for the latter family of planes. Again, these values are evidence of an expansion in the structure provoked by the inclusion of Bi into the lattice, which is reflected in the 7.8 and 4.2% expansions of the (200) and (111) planes (standard values are 2.04 and 2.36 Å for (200) and (111), respectively). In addition, a change in the angles between these planes was detected, where a slight deviation of 1.8−3.0% is observed from the ideal values. The EDS analysis in region 3 at the core

DOI: 10.1021/acsomega.8b01264
ACS Omega 2018, 3, 9880−9887

of the particle (Figure 4h) shows a slight decrease in the elemental percentage of Bi (96 ± 1 and 4 ± 1 atom % for Ag and Bi, respectively). Moreover, as shown in the HR-TEM image shown in Figure 4i, the (111) interplanar distance has increased (2.43 Å) compared to the reference value, but to a lesser extent than the value obtained at the border of the Ag−Bi NA. These behaviors are associated with the tendency of Bi to be located more at the boundaries of the Ag−Bi NA.

The EDS analysis clearly shows the presence of Ag (94 ± 1 to 96 ± 1 atom %) and Bi (4 ± 1 to 6 ± 1 atom %) at levels that indicate a higher miscibility of Bi in the Ag structure than that expected for Ag−Bi systems.[23] Moreover, despite the drawbacks predicted by the Hume-Rothery rules,[24] the present results show that the high energy provided by fs laser irradiation is able to stabilize an NA composed of Bi atoms inserted into the cubic Ag structure.

In the present study, as a novel application of this NA, the bactericidal activities of Bi and Ag NPs as well as the Ag−Bi NA were analyzed. In previous works, Ag-rich alloyed NPs, such as those containing Au, Cu, or Pt, demonstrated superior bactericidal properties.[48−50] Although recent studies have also shown that Bi inhibits some parasitic and microbial growth[51−53] and that the addition of Bi could modify the final properties of other alloys,[54,55] to the best of our knowledge, the bactericidal activity of Ag−Bi NAs has not been studied yet.

A strong inhibition of methicillin-resistant and methicillin-susceptible *S. aureus* bacteria (MRSA and MSSA, respectively) has been observed for both Ag NPs and Ag−Bi alloyed NPs. The minimum inhibitory concentration (MIC) found to be effective against MRSA was the same for both Ag^0 and Ag−Bi systems (3.91 μg/mL). For the susceptible strain, Ag^0 (1.95 μg/mL) was slightly more efficient than the Ag−Bi NA (3.91 μg/mL). Although Bi^0 NPs showed no antibacterial activity against any of the strains tested, when Bi atoms are associated with Ag, an MIC similar to that of pure Ag NPs was found. Moreover, the Ag−Bi system has a high antimicrobial efficiency compared to other Ag-rich alloys acting against similar microorganisms.[56] Figure 5 shows the micrographs acquired by confocal laser scanning microscopy (CLSM) of living MSSA and MRSA cells treated with the fs laser-irradiated materials. It is possible to observe large numbers of living cells (green) when treated with Bi NPs (Figure 5a,d). On the other hand, significant reductions in the number of live cells were observed for both bacteria when treated with Ag NPs (Figure 5b,e) and Ag−Bi alloyed NPs (Figure 5c,f). Hence, Ag−Bi NA possesses high antibacterial activity, but the solubilization of Bi into the Ag structure did not cause significant differences in the antibacterial activity against MRSA and MSSA compared to pure Ag^0, which supports the calculated MIC results. Ag NPs are known for their high antibacterial activity, but at certain concentrations, they are cytotoxic to human cells.[57] In contrast, Bi is biocompatible and presents great potential in biomedical procedures, such as radiosensitizers in antitumor treatments.[58] Thus, the high antibacterial activity of Ag−Bi NA demonstrated in this work, combined with both the biological properties of Bi and the new possible properties arising from synergistic effects between Ag and Bi could be interesting for future technological and biomedical approaches. Hence, the results here have the potential to further increase the range of applicability of Ag−Bi system alloyed at nanoscale.

In summary, bimetallic nanoalloys have abundant applications, but a thorough knowledge of the fundamentals of fs laser interactions with the target material is necessary to control their structure and properties. A new Ag−Bi NA with high bactericidal activity was prepared by fs laser irradiation. TEM, HR-TEM, STEM, and EDS analyses (local, line, and mapping) demonstrated the insertion of Bi atoms into the fcc Ag structure at concentrations of up to 6 ± 1 atom % at the surface and 4 ± 1 atom % at the core of the alloyed NPs. The results presented here expand the fundamental understanding of the atomic processes, which underpin the mechanics of Ag−Bi NA formation. Thus, the quantum phenomena associated with the fs irradiation, at the nanoscale, are able to minimize the difficulties involved in alloying metals that are very immiscible at the bulk scale, such as Ag and Bi. It was found that alloying Ag and Bi at the atomic level leads to a high antibacterial activity against MSSA and MRSA cells (MIC = 3.91 μg/mL). More broadly, this research introduces a new strategy for producing Ag−Bi NAs using complex inorganic oxides as precursors as well as a new candidate in the pool of binary nanoalloys formed from elements that are immiscible at the bulk scale. It is anticipated that the obtained Ag−Bi NAs will also find further applications as effective biomedical devices and catalysts.

3. EXPERIMENTAL SECTION

3.1. Materials. Sodium tungstate dihydrate ($Na_2WO_4 \cdot 2H_2O$, 99%, Sigma-Aldrich), silver nitrate ($AgNO_3$, 99%, Sigma-Aldrich), and sodium bismuthate ($NaBiO_3$, 80%, Alfa-Aesar) were used as starting precursors.

3.2. Synthesis of α-Ag_2WO_4 Microrods. α-Ag_2WO_4 powders were prepared in accordance with the procedure described by Longo et al.[39] Briefly, 1.0 mmol of $Na_2WO_4 \cdot 2H_2O$ and 2.0 mmol of $AgNO_3$ were dissolved separately in 50 mL of deionized water. Then, both the solutions were heated to 90 °C and kept under vigorous stirring. The $AgNO_3$ solution was transferred into the other solution. Once the solutions were well mixed, the gray suspension thus formed was continuously stirred for 10 min at 90 °C. The obtained crystals were allowed to precipitate at the bottom of the flask by turning off the magnetic stirring and naturally cooled to ambient temperature. The precipitate was separated by centrifugation and then washed with deionized water and acetone to remove any remaining impurities or reaction byproducts. The crystals were dried in an oven at 60 °C for 12 h.

3.3. Preparation of α-Ag_2WO_4/$NaBiO_3$. For the preparation of the α-Ag_2WO_4/$NaBiO_3$ precursor, the α-Ag_2WO_4 powders previously synthesized by chemical precipitation were combined with a commercial $NaBiO_3$ precursor by mechanical grinding. In this procedure, the α-Ag_2WO_4 and $NaBiO_3$ powders were homogeneously mixed in an agate mortar at a molar ratio of 50:50 and ground for 15 min.

3.4. Synthesis of Ag−Bi Nanoalloys by Femtosecond Laser Irradiation. α-Ag_2WO_4, $NaBiO_3$, and Ag_2WO_4/$NaBiO_3$ powders were irradiated with a Ti:sapphire laser (Femtopower Compact Pro, Femto Lasers) using 30 fs full width at half-maximum (FWHM) pulses at a central wavelength of 800 nm and a repetition rate of 1 kHz. A laser beam with a mean power of 200 mW was focused onto the surface of the target powder with a spherical convex lens of 75 mm focal length to obtain a focal spot with a diameter of 20.6 μm FWHM. The α-Ag_2WO_4, $NaBiO_3$, and Ag_2WO_4/$NaBiO_3$ samples were placed at the bottom of a quartz cuvette attached to a two-dimensional motion-controlled stage moving

DOI: 10.1021/acsomega.8b01264
ACS Omega 2018, 3, 9880−9887

at a constant speed of 0.45 mm/s in the focus plane perpendicular to the laser beam in a stairlike pattern. A programmable acousto-optic filter (Fazzler, Faslite) was utilized to obtain a more precise pulse compression at the target substrate. The monometallic and bimetallic alloyed NPs obtained in the plasma plume by irradiating the α-Ag_2WO_4, $NaBiO_3$, and α-Ag_2WO_4/$NaBiO_3$ targets were recovered for further morphological and structural characterization as well as to probe their biological activities.

3.5. Characterization. The samples were structurally characterized by X-ray diffraction in a Rigaku D/Max-2500PC (Japan) diffractometer using Cu Kα radiation (λ = 0.15406 nm). Data were collected over 2θ ranging from 20 to 70°, and at a step scan rate and step size of 1°/min and 0.02°, respectively. The morphological features were examined by field-emission scanning electron microscopy (FE-SEM) with a Carl Zeiss Supra 35-VP (Germany) microscope operated at 5 kV. Transmission electron microscopy (TEM), high-resolution TEM (HR-TEM), energy-dispersive X-ray spectroscopy (EDS) analysis as well as scanning transmission electron microscopy (STEM) were performed with an FEI Tecnai F20 (The Netherlands) microscope operating at 200 kV. To analyze the metallic species readily formed in the plasma plume by electron microscopy, we recollected free-flying particles using a TEM grid before the formation of deposits in the bottom of the sample flask. This procedure avoids other variables in NPs characterization by TEM, such as the necessity of redispersion of NPs in a solvent to prepare the samples for analyses. It is important to mention that more than 10 HR-TEM images and EDS analyses of different zones of Ag−Bi NPs were realized during the EM characterization to describe the Ag−Bi sample. Processing of the micrographs was carried out using DigitalMicrograph (Gatan) software. The dimensions of the nanoparticles were estimated using distinct TEM images collected from the irradiated sample and analyzed with ImageJ (NIH) software; the number of counts required for statistical analysis was 150 nanoparticles.

3.6. Bactericidal Activity. The microdilution method for planktonic cells was carried out to determine the minimum inhibitory concentration (MIC) against bacterial strains, according to Clinical Laboratory Standards Institute protocols with modifications.[59] For bactericidal probes, the Bi, Ag, and Ag−Bi NPs generated in the plasma plume were analyzed by recovering the particles allowed to settle down in the form of a thin layer at the bottom of the samples flasks. The Bi, Ag, and Ag−Bi samples were resuspended in a sterile tryptic soy broth (TSB) culture medium at the required concentrations of 1000−0.49 μg/mL, using the serial 2-fold dilution method. Standard strains of methicillin-resistant (MRSA) and methicillin-susceptible (MSSA) *S. aureus* from the American Type Culture Collection were used in this study. The microorganisms were stored at −80 °C in TSB with glycerol prior to the experiments. Strains were plated on Mueller-Hinton agar plates and incubated at 37 °C for 24 h. Then, MSSA and MRSA cells were grown in TSB up to the mid-exponential phase of growth. MICs were determined by incubating microorganisms on a 96-well microtiter plate exposed to serial dilution of the materials suspensions for 24 h at 37 °C. The structural organization of the MSSA and MRSA culture cells treated by the nanoalloys was analyzed by laser scanning confocal microscopy. For this purpose, the bacteria cells were labeled with SYTO9 and propidium iodide (kit Live/Dead BacLight Molecular Probes Inc., Eugene, OR) after treatment with the nanoalloys. The confocal imaging was performed using a Carl Zeiss LSM 800 microscope.

■ ASSOCIATED CONTENT

Supporting Information

The Supporting Information is available free of charge on the ACS Publications website at DOI: 10.1021/acsomega.8b01264.

Characterization of precursor targets and Ag^0 and Bi^0 NPs (PDF)

■ AUTHOR INFORMATION

Corresponding Author

*E-mail: elson.liec@gmail.com.

ORCID

Marcelo Assis: 0000-0003-0355-5565
Carlos Doñate-Buendia: 0000-0002-7022-0960
Camila C. Foggi: 0000-0002-1210-1234
Héctor Beltrán-Mir: 0000-0002-7836-1602
Juan Andrés: 0000-0003-0232-3957
Elson Longo: 0000-0001-8062-7791

Author Contributions

The manuscript was written through contributions of all authors. All authors have given approval to the final version of the manuscript.

Notes

The authors declare no competing financial interest.

■ ACKNOWLEDGMENTS

The authors are grateful to CAPES/PNPD, CEPID-FAPESP (2013/07296-2), FAPESP (2017/12594-3), CNPq (150205/2017-1), Ministerio de Economia y Competitividad (MAT2016-80410-P, FIS2016-75618-R and CTQ2015-65207-P), Universitat Jaume I (UJI-B2016-38 and UJI-B2016-25), Generalitat Valenciana (PROMETEU/2016/079 and ACOMP/2015/1202) for the financial support. The authors are also very grateful to the Serveis Centrals d'Instrumentació Cientifica (SCIC) of the University Jaume I for the use of the femtosecond laser and microscopy facilities. Special thanks go to Dr. Saïd Agouram, Rorivaldo Camargo, and João P. C. Costa for their scientific and technical support. The authors also thank Enio Longo for design contributions.

■ REFERENCES

(1) Jellinek, J. Nanoalloys: Tuning Properties and Characteristics through Size and Composition. *Faraday Discuss.* **2008**, *138*, 11−35.
(2) Ferrando, R.; Jellinek, J.; Johnston, R. L. Nanoalloys: From Theory to Applications of Alloy Clusters and Nanoparticles. *Chem. Rev.* **2008**, *108*, 845−910.
(3) Singh, A. K.; Xu, Q. Synergistic Catalysis over Bimetallic Alloy Nanoparticles. *ChemCatChem* **2013**, *5*, 652−676.
(4) Shi, J. On the Synergetic Catalytic Effect in Heterogeneous Nanocomposite Catalysts. *Chem. Rev.* **2013**, *113*, 2139−2181.
(5) Mun, J. H.; Chang, Y. H.; Shin, D. O.; Yoon, J. M.; Choi, D. S.; Lee, K. M.; Kim, J. Y.; Cha, S. K.; Lee, J. Y.; Jeong, J. R.; et al. Monodisperse Pattern Nanoalloying for Synergistic Intermetallic Catalysis. *Nano Lett.* **2013**, *13*, 5720−5726.
(6) Pang, H.; Gallou, F.; Sohn, H.; Camacho-Bunquin, J.; Delferro, M.; Lipshutz, B. H. Synergistic Effects in Fe Nanoparticles Doped with ppm Levels of (Pd + Ni). A New Catalyst for Sustainable Nitro Group Reductions. *Green Chem.* **2018**, *20*, 130−135.

DOI: 10.1021/acsomega.8b01264
ACS Omega 2018, 3, 9880−9887

(7) Cabrero-Antonino, J. R.; Tejeda-Serrano, M.; Quesada, M.; Vidal-Moya, J. A.; Leyva-Pérez, A.; Corma, A. Bimetallic Nanosized Solids with Acid and Redox Properties for Catalytic Activation of C−C and C−H Bonds. *Chem. Sci.* **2017**, *8*, 689−696.
(8) Yu, F.; Zhou, W.; Bellabarba, R. M.; Tooze, R. P. One-Step Synthesis and Shape-Control of CuPd Nanowire Networks. *Nanoscale* **2014**, *6*, 1093−1098.
(9) Zhang, H.; Son, J. S.; Jang, J.; Lee, J. S.; Ong, W. L.; Malen, J. A.; Talapin, D. V. $Bi_{1-x}Sb_x$ Alloy Nanocrystals: Colloidal Synthesis, Charge Transport, and Thermoelectric Properties. *ACS Nano* **2013**, *7*, 10296−10306.
(10) Yamauchi, M.; Okubo, K.; Tsukuda, T.; Kato, K.; Takata, M.; Takeda, S. Hydrogen-Induced Structural Transformation of AuCu Nanoalloys Probed by Synchrotron X-Ray Diffraction Techniques. *Nanoscale* **2014**, *6*, 4067−4071.
(11) Coq, B.; Figueras, F. Bimetallic Palladium Catalysts: Influence of the Co-Metal on the Catalyst Performance. *J. Mol. Catal. A: Chem.* **2001**, *173*, 117−134.
(12) Gaudry, M.; Cottancin, E.; Pellarin, M.; Lermé, J.; Arnaud, L.; Huntzinger, J. R.; Vialle, J. L.; Broyer, M.; Rousset, J. L.; Treilleux, M.; et al. Size and Composition Dependence in the Optical Properties of Mixed (Transition Metal/noble Metal) Embedded Clusters. *Phys. Rev. B* **2003**, *67*, No. 155409.
(13) Paulus, U. A.; Wokaun, A.; Scherer, G. G.; Schmidt, T. J.; Stamenkovic, V.; Radmilovic, V.; Markovic, N. M.; Ross, P. N. Oxygen Reduction on Carbon-Supported Pt-Ni and Pt-Co Alloy Catalysts. *J. Phys. Chem. B* **2002**, *106*, 4181−4191.
(14) Son, S. U.; Jang, Y.; Park, J.; Na, H.; Park, H. M.; Yun, H. J.; Lee, J.; Hyeon, T. Designed Synthesis of Atom-Economical Pd/Ni Bimetallic Nanoparticle-Based Catalysts for Sonogashira Coupling Reactions. *J. Am. Chem. Soc.* **2004**, *126*, 5026−5027.
(15) Cao, Y.; Jin, R.; Mirkin, C. A. DNA-Modified Core-Shell Ag/Au Nanoparticles. *J. Am. Chem. Soc.* **2001**, *123*, 7961−7962.
(16) Guo, S.; Wang, E. Functional Micro/nanostructures: Simple Synthesis and Application in Sensors, Fuel Cells, and Gene Delivery. *Acc. Chem. Res.* **2011**, *44*, 491−500.
(17) Burda, C.; Chen, X.; Narayanan, R.; El-Sayed, M. A. Chemistry and Properties of Nanocrystals of Different Shapes. *Chem. Rev.* **2005**, *105*, 1025−1102.
(18) Ferrando, R. *Structure and Properties of Nanoalloys*; Elsevier: Amsterdam, 2016.
(19) Christensen, A.; Stoltze, P.; Norskov, J. K. Size Dependence of Phase Separation in Small Bimetallic Clusters. *J. Phys.: Condens. Matter* **1995**, *7*, 1047−1057.
(20) Toshima, N.; Wang, Y. Preparation and Catalysis of Novel Colloidal Dispersions of Copper/Noble Metal Bimetallic Clusters. *Langmuir* **1994**, *10*, 4574−4580.
(21) Zlotea, C.; Morfin, F.; Nguyen, T. S.; Nguyen, N. T.; Nelayah, J.; Ricolleau, C.; Latroche, M.; Piccolo, L. Nanoalloying Bulk-Immiscible Iridium and Palladium Inhibits Hydride Formation and Promotes Catalytic Performances. *Nanoscale* **2014**, *6*, 9955−9959.
(22) Digges, T. G.; Tauber, R. N. Structure of Bi-Ag Eutectic Alloy. *J. Cryst. Growth* **1971**, *8*, 132−134.
(23) Karakaya, I.; Thompson, W. T. The Ag-Bi (Silver-Bismuth) System. *J. Phase Equilib.* **1993**, *14*, 525−530.
(24) Hume-Rothery, W.; Haworth, C. W.; Smallman, R. E. *The Structure of Metals and Alloys*; Institute of Metals and the Institution of Metallurgists: London, 1969.
(25) Jiao, Z.; Zhang, Y.; Ouyang, S.; Yu, H.; Lu, G.; Ye, J.; Bi, Y. BiAg Alloy Nanospheres: A New Photocatalyst for H_2 Evolution from Water Splitting. *ACS Appl. Mater. Interfaces* **2014**, *6*, 19488−19493.
(26) Gong, J.; Lee, C.; Chang, Y.; Chang, Y. A Novel Self-Assembling Nanoparticle of Ag−Bi with High Reactive Efficiency. *Chem. Commun.* **2014**, *50*, 8597−8600.
(27) Ruiz-Ruiz, V.-F.; Zumeta-Dubé, I.; Díaz, D.; Arellano-Jiménez, M. J.; José-Yacamán, M. Can Silver Be Alloyed with Bismuth on Nanoscale? An Optical and Structural Approach. *J. Phys. Chem. C* **2017**, *121*, 940−949.
(28) Vorobyev, A. Y.; Guo, C. Direct Femtosecond Laser Surface Nano/microstructuring and Its Applications. *Laser Photonics Rev.* **2013**, *7*, 385−407.
(29) Xiong, W.; Zhou, Y.; Hou, W.; Jiang, L.; Mahjouri-Samani, M.; Park, J.; He, X.; Gao, Y.; Fan, L.; Baldacchini, T.; et al. Laser-Based Micro/nanofabrication in One, Two and Three Dimensions. *Front. Optoelectron.* **2015**, *8*, 351−378.
(30) Tan, D.; Zhou, S.; Qiu, J.; Khusro, N. Preparation of Functional Nanomaterials with Femtosecond Laser Ablation in Solution. *J. Photochem. Photobiol., C* **2013**, *17*, 50−68.
(31) Nandini, P.; Akash, K.; Rohit, G.; Vipul, S.; Palani, I. A. Investigations on the Influence of Liquid-Assisted Laser Ablation of NiTi Rotating Target to Improve the Formation Efficiency of Spherical Alloyed NiTi Nanoparticles. *J. Mater. Eng. Perform.* **2017**, *26*, 4707−4717.
(32) Chen, Q.; Song, H.; Zhang, F.; Zhang, H.; Yu, Y.; Chen, Z.; Wei, R.; Dai, Y.; Qiu, J. A Strategy for Fabrication of Controllable 3D Pattern Containing Clusters and Nanoparticles inside a Solid Material. *Nanoscale* **2017**, *9*, 9083−9088.
(33) Fujita, Y.; Aubert, R.; Walke, P.; Yuan, H.; Kenens, B.; Inose, T.; Steuwe, C.; Toyouchi, S.; Fortuni, B.; Chamtouri, M.; et al. Highly Controllable Direct Femtosecond Laser Writing of Gold Nanostructures on Titanium Dioxide Surfaces. *Nanoscale* **2017**, *9*, 13025−13033.
(34) Sarker, M. S. I.; Nakamura, T.; Herbani, Y.; Sato, S. Fabrication of Rh Based Solid-Solution Bimetallic Alloy Nanoparticles with Fully-Tunable Composition through Femtosecond Laser Irradiation in Aqueous Solution. *Appl. Phys. A: Mater. Sci. Process.* **2013**, *110*, 145−152.
(35) Assis, M.; Cordoncillo, E.; Torres-Mendieta, R.; Beltrán-Mir, H.; Mínguez-Vega, G.; Oliveira, R.; Leite, E. R.; Foggi, C. C.; Vergani, C. E.; Longo, E.; et al. Towards Scale-up the Formation of Nanoparticles on α−Ag_2WO_4 with Bactericide Properties by Femtosecond Laser Irradiation. *Sci. Rep.* **2018**, *8*, No. 1884.
(36) Chau, J. L. H.; Chen, C. Y.; Yang, C. C. Facile Synthesis of Bimetallic Nanoparticles by Femtosecond Laser Irradiation Method. *Arabian J. Chem.* **2017**, *10*, S1395−S1401.
(37) Zhang, D.; Gökce, B.; Barcikowski, S. Laser Synthesis and Processing of Colloids: Fundamentals and Applications. *Chem. Rev.* **2017**, *117*, 3990−4103.
(38) Longo, V. M.; Foggi, C.; Ferrer, M. M.; Gouveia, A. F.; André, R. S.; Avansi, W.; Vergani, C. E.; Machado, A. L.; Andrés, J.; Hernandes, A. C.; et al. Potentiated Electron Transference in α-Ag_2WO_4 Microcrystals with Ag Nanofilaments as Microbial Agent. *J. Phys. Chem. A* **2014**, *118*, 5769−5778.
(39) Longo, E.; Volanti, D. P.; Longo, V. M.; Gracia, L.; Nogueira, I. C.; Almdeira, M. A. P.; Pinheiro, A. N.; Ferrer, M. M.; Cavalcante, L. S.; Andrés, J. Toward an Understanding of the Growth of Ag Filaments on α-Ag_2WO_4 and Their Photoluminescent Properties: A Combined Experimental and Theoretical Study. *J. Phys. Chem. C* **2014**, *118*, 1229−1239.
(40) de Oliveira, R. C.; Zanetti, S. M.; Assis, M.; Penha, M.; Mondego, M.; Cilense, M.; Longo, E.; Cavalcante, L. S. Effect of Metallic Ag Growth on the Electrical Resistance of 3D Flower-like $Ag_4V_2O_7$ Crystals. *J. Am. Ceram. Soc.* **2017**, *100*, 2358−2362.
(41) Longo, E.; Cavalcante, L. S.; Volanti, D. P.; Gouveia, A. F.; Longo, V. M.; Varela, J. A.; Orlandi, M. O.; Andrés, J. Direct in Situ Observation of the Electron-Driven Synthesis of Ag Filaments on α-Ag_2WO_4 Crystals. *Sci. Rep.* **2013**, *3*, No. 1676.
(42) Andrés, J.; Gracia, L.; Gonzalez-Navarrete, P.; Longo, V. M.; Avansi, W. J.; Volanti, D. P.; Ferrer, M. M.; Lemos, P. S.; La Porta, F. A.; Hernandes, A. C.; et al. Structural and Electronic Analysis of the Atomic Scale Nucleation of Ag on α-Ag_2WO_4 Induced by Electron Irradiation. *Sci. Rep.* **2014**, *4*, No. 5391.
(43) Longo, E.; Avansi, W. J.; Bettini, J.; Andrés, J.; Gracia, L. In Situ Transmission Electron Microscopy Observation of Ag Nanocrystal Evolution by Surfactant Free Electron-Driven Synthesis. *Sci. Rep.* **2016**, *6*, No. 21498.

DOI: 10.1021/acsomega.8b01264
ACS Omega 2018, 3, 9880−9887

(44) San-Miguel, M. A.; da Silva, E. Z.; Zanetti, S. M.; Cilense, M.; Fabbro, M. T.; Gracia, L.; Andrés, J.; Longo, E. *In Situ* Growth of Ag Nanoparticles on α-Ag_2WO_4 under Electron Irradiation: Probing the Physical Principles. *Nanotechnology* **2016**, *27*, No. 225703.
(45) Fabbro, M. T.; Gracia, L.; Silva, G. S.; Santos, L. P. S.; Andrés, J.; Cordoncillo, E.; Longo, E. Understanding the Formation and Growth of Ag Nanoparticles on Silver Chromate Induced by Electron Irradiation in Electron Microscope: A Combined Experimental and Theoretical Study. *J. Solid State Chem.* **2016**, *239*, 220−227.
(46) Assis, M.; Cordoncillo, E.; Torres-Mendieta, R.; Beltrán-Mir, H.; Minguez-Vega, G.; Gouveia, A. F.; Leite, E.; Andrés, J.; Longo, E. Laser-Induced Formation of Bismuth Nanoparticles. *Phys. Chem. Chem. Phys.* **2018**, 13693−13696.
(47) Wells, A. F. *Structural Inorganic Chemistry*; Clarendon Press: Oxford, 1984.
(48) Hu, X.; Zhao, Y.; Hu, Z.; Saran, A.; Hou, S.; Wen, T.; Liu, W.; Ji, Y.; Jiang, X.; Wu, X. Gold Nanorods core/AgPt Alloy Nanodots Shell: A Novel Potent Antibacterial Nanostructure. *Nano Res.* **2013**, *6*, 822−835.
(49) Paszkiewicz, M.; Gołąbiewska, A.; Rajski, Ł.; Kowal, E.; Sajdak, A.; Zaleska-Medynska, A. Synthesis and Characterization of Monometallic (Ag, Cu) and Bimetallic Ag-Cu Particles for Antibacterial and Antifungal Applications. *J. Nanomater.* **2016**, *2016*, No. 2187940.
(50) Padmos, J. D.; Langman, M.; Macdonald, K.; Comeau, P.; Yang, Z.; Filiaggi, M.; Zhang, P. Correlating the Atomic Structure of Bimetallic Silver Gold Nanoparticles to Their Antibacterial and Cytotoxic Activities. *J. Phys. Chem. C* **2015**, *119*, 7472−7482.
(51) Rodríguez-Luis, O. E.; Hernández-Delgadillo, R.; Pineda-Aguilar, N.; Vargas-Villarreal, J.; González-Salazar, F.; Garza-González, J. N.; Hernández-García, M. E.; Chellam, S.; Cabral-Romero, C. Effect of Bismuth Lipophilic Nanoparticles (BisBAL NPs) on *Trichomonas vaginalis* Growth. *J. Nanosci. Nanotechnol.* **2016**, *16*, 1−5.
(52) Badireddy, A. R.; Hernandez-Delgadillo, R.; Sánchez-Nájera, R. I.; Chellam, S.; Cabral-Romero, C. Synthesis and Characterization of Lipophilic Bismuth Dimercaptopropanol Nanoparticles and Their Effects on Oral Microorganisms Growth and Biofilm Formation. *J. Nanopart. Res.* **2014**, *16*, No. 2456.
(53) Hernandez-Delgadillo, R.; Del Angel-Mosqueda, C.; Solís-Soto, J. M.; Munguia-Moreno, S.; Pineda-Aguilar, N.; Sánchez-Nájera, R. I.; Chellam, S.; Cabral-Romero, C. Antimicrobial and Antibiofilm Activities of MTA Supplemented with Bismuth Lipophilic Nanoparticles. *Dent. Mater. J.* **2017**, *36*, 503−510.
(54) Gandhi, A. C.; Wu, S. Y. Routes to Probe Bismuth Induced Strong-Coupling Superconductivity in Bimetallic BiIn Alloys. *Sci. Rep.* **2017**, *7*, No. 9442.
(55) Polak, M. P.; Scharoch, P.; Kudrawiec, R. First-Principles Calculations of Bismuth Induced Changes in the Band Structure of Dilute Ga-V-Bi and In-V-Bi Alloys: Chemical Trends versus Experimental Data. *Semicond. Sci. Technol.* **2015**, *30*, No. 094001.
(56) Grade, S.; Eberhard, J.; Jakobi, J.; Winkel, A.; Stiesch, M.; Barcikowski, S. Alloying Colloidal Silver Nanoparticles with Gold Disproportionally Controls Antibacterial and Toxic Effects. *Gold Bull.* **2014**, *47*, 83−93.
(57) Franci, G.; Falanga, A.; Galdiero, S.; Palomba, L.; Rai, M.; Morelli, G.; Galdiero, M. Silver Nanoparticles as Potential Antibacterial Agents. *Molecules* **2015**, *20*, 8856−8874.
(58) Deng, J.; Xu, S.; Hu, W.; Xun, X.; Zheng, L.; Su, M. Tumor Targeted, Stealthy and Degradable Bismuth Nanoparticles for Enhanced X-Ray Radiation Therapy of Breast Cancer. *Biomaterials* **2018**, *154*, 24−33.
(59) Clinical and Laboratory Standards Institute (CLSI). *M27−A: Performance Standards for Antimicrobial Susceptibility Testing*; CLSI: Villanova, PA, 1997.

DOI: 10.1021/acsomega.8b01264
ACS Omega 2018, 3, 9880−9887